33rd Annual International Conference of the IEEE EMBS
Boston, Massachusetts USA, August 30 - September 3, 2011

Experimental Validation of Alternating Transillumination for Imaging Intramural Wave Propagation

Richard D. Walton, Christopher D. Lawrence Xavier, Ilias Tachtsidis, and Olivier Bernus

Abstract— **Current techniques to map intramural activation patterns in *ex vivo* cardiac tissue have limited spatial resolution. Here, we report on the experimental validation of a novel optical technique that was recently proposed to resolve the size and depth of intramural wave fronts using alternating transillumination (AT). AT was achieved by simultaneously mapping the epi- and endocardial surfaces with two synchronized CCD cameras and rapidly alternating LED illumination between both surfaces. Optical phantoms were made based on tissue optical properties measured using a hybrid optical spectrometer. Spherical fluorescent sources (Scarlet microspheres, Invitrogen, UK) of varying sizes were embedded at known depths in the phantoms. Coronary-perfused procine left ventricular slab preparations were stained with DI-4-ANBDQBS (n=3) and paced at known intramural depths. In phantoms we were able to reliably estimate the depth of the center of fluorescent sources (9.6±5.4% error), as well as their transmural extent (15.7±11.5% error). In ventricular slabs we were able to localize the sites of origin of intramural excitation waves with a precision of ±1.6 mm. Transmural conduction velocities were, for the first time, measured optically from the surfaces and found to be 21.0±12.4 cm/s. In conclusion, alternating transillumination is a promising technique for reliable reconstruction of depth and expansion rate of intramural activation wave fronts in cardiac tissue.**

I. INTRODUCTION

DISRUPTION to the normal electrical activation of the heart, can lead to dangerous arrhythmias such as ventricular fibrillation (VF), which can result in sudden cardiac death. VF is characterised by chaotic electrical activity within the ventricles [1]. The initiation of idiopathic VF has been attributed to the occurrence of focal, ectopic activity and the use of targeted radiofrequency (RF) catheter ablation of sites susceptible to ectopic activity has proven to be an effective therapy to arrest idiopathic VF and prevent its recurrence [2]. However, localizing the three-dimensional site of origin remains problematic for intramural foci even in *ex vivo* cardiac tissue preparations. Furthermore, the complexity of the activation sequence during VF and the limited intramural resolutions achievable with conventional methods, are such that the underlying mechanisms for the initiation and maintenance of VF are still a matter of debate [1].

Current techniques to map intramural activation patterns in isolated hearts or cardiac tissue preparations have limited in-plane spatial resolution and/or require plunge electrodes[3], optrodes [4] or optical imaging from exposed transmural cut surfaces [5]. However, a recent computational study provided the proof-of-principle for a novel optical imaging technique to accurately resolve the size and depth of intramural wave fronts from surface images [6]. This technique is based on the use of alternating transillumination (AT) in which reflection and transillumination fluorescence images are obtained simultaneously from the epi- and endocardial surfaces of ventricular wedge preparations. The ratio of the spatially integrated reflection and transillumination images was shown, *in silico*, to yield the accurate depth and transmural thickness of intramural fluorescent sources. A recent experimental study provided a first step in the validation of this novel method by showing that it can accurately reconstruct the location of intramural ectopic sources in coronary-perfused porcine ventricular preparations [7]. However, the full potential of AT in also reconstructing the transmural extent of the wave and its propagation velocity have yet to be explored. Here, we report on the first experimental validation for measuring the transmural extent of intramural waves and their conduction velocities.

II. METHODS

A. Hybrid Optical Spectrometry

In order to create optical phantoms relevant for cardiac tissue at the wavelengths of interest, we measured the optical properties of porcine ventricles using a hybrid optical spectrometer (pHOS) [8]. Briefly, female pigs (25-27 kg, n=2) were euthanized with sodium pentobarbital (35 mg/kg) and the hearts were quickly excised. The aorta was cannulated and perfused with cold cardioplegic solution containing (in mM): glucose, 277.5; KCl, 30; $NaHCO_3$, 25; mannitol, 34.3, and supplemented with heparin (5 U/ml). Measurements were taken from various locations of the epicardium (n=7). pHOS uses a multi-distance frequency domain (MDFD) system to measure the absorption coefficient (μ_a) and the reduced scattering coefficient (μ_s')

Manuscript received March 25, 2011. This work was supported in part by the EPSRC under grant EP/F065574/1.

R. D. Walton, C. D. Lawrence Xavier and O. Bernus are with the faculty of Biological Sciences, Multidisciplinary Cardiovascular Research Centre, University of Leeds, Leeds, LS2 9JT UK (r.d.walton@leeds.ac.uk, chriz991@gmail.com and o.bernus@leeds.ac.uk).

O.Bernus is also with the Institut de Rhytmologie et Modelisation Cardiaque, Université Bordeaux Segalen, Centre, Hospitalier Universitaire de Bordeaux, Hôpital Haut-Lévêque, Avenue de Magellan, 33604, Pessac Cedex, France.

I. Tachtsidis is with the Department of Medical Physics & Bioengineering, Malet Place Eng. Bldg., University College London, Gower St., London WC1E 6BT, UK (iliastac@medphys.ucl.ac.uk).

of tissue at a selection of discrete wavelengths and assumes a power law wavelength dependence of scattering to interpolate and extrapolate μ_s' over all wavelengths in the spectral window. Furthermore, it uses a multi-distance broadband spectrometer (MDBBS) to measure the attenuation slope at a number of source detector spacings and to provide spatially resolved measures of μ_a and μ_s'. Here, we were particularly interested in the 650-700 nm and 700-800 nm spectral windows as these correspond to the excitation and emission windows of the voltage-sensitive dye utilized in this study (see below). The measured optical parameters and calculated optical attenuation lengths δ are shown in Table I.

TABLE I
OPTICAL PROPERTIES OF PORCINE VENTRICULAR MYOCARDIUM

	μ_a(cm^{-1})	μ_s'(cm^{-1})	δ (cm)
650-700 nm	0.32±0.22	8.99±2.51	0.40 ± 0.12
700-800 nm	0.21±0.04	6.70±1.75	0.50 ± 0.07

B. Optical Phantoms

Optical phantoms were designed to mimic the measured optical properties of ventricular myocardium. Gelatin-based phantoms (10%) were supplemented with Indian ink (0.53 ml/l) and Intralipid (24.0 ml/l) to yield an attenuation length of 0.48 cm at 715 nm. The phantom media was set in a 100x150x20 mm perspex cast. Sylgard-based fluorescent inclusions were made by mixing the phantom medium with scarlet fluorescent microspheres ($5x10^4$ microspheres/ml, Scarlet, Invitrogen, UK). Spherical fluorescent inclusions were cast with transmural thicknesses ranging from 4-12 mm and incorporated into the phantom at various depths ranging from 6-14 mm.

C. Porcine Left-Ventricular Wedge Preparations

Female pigs (25-27 kg, n=3) were euthanized with sodium pentobarbital (35 mg/kg) and the hearts were quickly excised. The aorta was cannulated and perfused with cold cardioplegic solution supplemented with heparin (5 U/ml). The left ventricular wall was dissected and the left anterior descending coronary artery was cannulated and perfused with bicarbonate buffered saline solution containing (mM): NaCl, 130; $NaHCO_3$, 24; NaH_2PO_4, 1.2; $MgCl_2$, 1; glucose, 5.6; KCl, 4; $CaCl_2$; oxygenated with 95% O_2/5% CO_2, pH 7.4, 37 °C. The perfusate was supplemented with blebbistatin (10 μM) to inhibit contraction and associated motion artefacts. The tissue was stained with the near-infrared potentiometric dye DI-4-ANBDQBS (0.15 μg/ml in the bicarbonate saline solution) via the perfusate at the beginning of the experiment. Bipolar plunge electrodes were used to stimulate the ventricles intramurally at 3 Hz at either 5 or 8 mm from the epicardial surface. Mean tissue thicknesses measured at the end of each experiment were 14.3±1.4 mm.

D. Optical Imaging

Phantoms or ventricular wedges were positioned between two high-frame-rate CCD video cameras (SciMeasure Analytical systems, GA, USA) mounted with lenses (focal length 12 mm, 1:0.8 aperture ratio; Computar, London, UK) simultaneously recording 2D optical images from the epicardial (P) and endocardial (N) surfaces. Epicardial and endocardial surfaces were alternately illuminated using monochromatic 660 nm LEDs (Cairn Research Ltd, Kent, UK) by software-triggered TTL signals (1.5 kHz) synchronous with half the acquisition rate. TTL signals spanned two frames to allow for LED flux decay between frames yielding an effective frame rate of 750 Hz. This generated 4 optical images, reflection and transillumination during both epicardial and endocardial illumination modalities (Fig. 1). We denote these four images as PP, PN, NP, and NN. The first letter refers to the surface that is illuminated, while the second refers to the imaged surface [7]. For example: PP means that fluorescence was recorded from the epicardium in reflection mode, whereas PN indicates transillumination with acquisition from the endocardium. Emission light was filtered through a long-pass 715 nm filter. Images (40x40 pixels) with pixel dimensions of 1x1mm were acquired.

In the phantom experiments, optical images were averaged over an acquisition period of 1 second, background subtracted and normalised to account for non-uniform illumination of the imaged surface. In the tissue experiments, optical action potentials acquired over a period of 10 seconds were aligned according to stimulation time and ensemble averaged followed by temporal (1.5 ms kernel) and spatial (3 mm kernel) filtration. Background fluorescence, obtained during diastole, was subtracted and used for normalization of optical signals to account for non-uniform illumination of the imaged surface, as previously described.

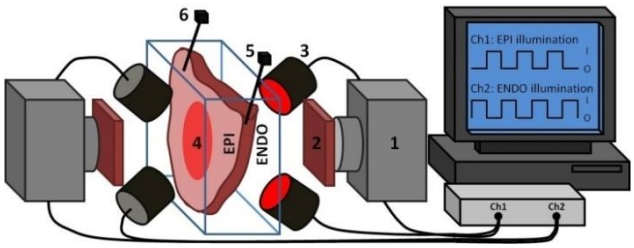

Fig. 1: Schematic representation of the optical imaging setup: (1) CCD camera, (2) emission filter, (3) LED illuminator, (4) tissue sample, (5) ECG electrode, (6) bipolar stimulating electrode.

E. Depth Detection Algorithm

The localization and transmural extent of intramural waves are derived using a method described in [6]. Briefly, The ratio of total signals from the reflected and transilluminated images for both epicardial ($\boldsymbol{J}_{PP}$ and $\boldsymbol{J}_{PN}$ respectively) and endocardial ($\boldsymbol{J}_{NN}$ and $\boldsymbol{J}_{NP}$ respectively) illumination is used:

$$\frac{\boldsymbol{J}_{PP}}{\boldsymbol{J}_{PN}} = \frac{\sinh\left[\left(L - Z_P + d\right)/\delta\right]}{\sinh\left[\left(Z_P + d\right)/\delta\right]} \qquad (1)$$

$$\frac{\boldsymbol{J}_{NN}}{\boldsymbol{J}_{NP}} = \frac{\sinh\left[\left(L - Z_N + d\right)/\delta\right]}{\sinh\left[\left(Z_N + d\right)/\delta\right]} \qquad (2)$$

Where L is the thickness of tissue, d is the extrapolation distance for incident light and δ is the emission attenuation length. Z_P and Z_N denote the distance of the wave front from the epi- and endocardial surfaces respectively and are obtained by solutions of Eqs. (1-2) and an iterative scheme as described in [6]. The centre of mass of the expanding wave front, Z_C, is obtained as the mean of Z_P and Z_N. The origin of excitation is determined through linear regression of the expanding wave front. Mean transmural conduction velocities are determined from Z_P and Z_N estimated from adjacent frames throughout the optical upstroke.

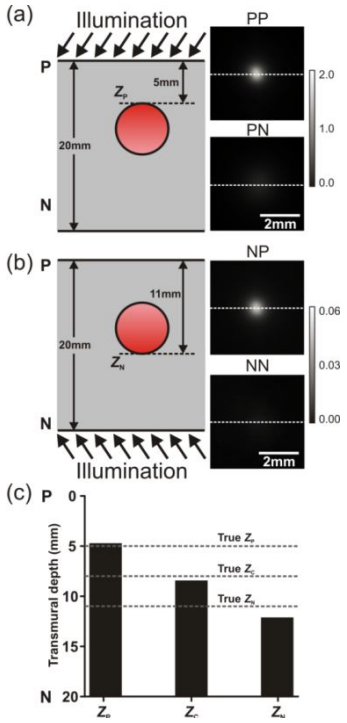

Fig. 2: Alternating illumination of the "epicardial" (a) and "endocardial" (b) surface of an optical phantom containing a fluorescent sphere at 8 mm depth. Panel (c) shows the reconstructed depths Z_P, Z_C and Z_N.

III. Results

A. Depth detection in optical phantoms

Fig. 2 illustrates the technique for a fluorescent sphere of 6 mm diameter with its centre at 8 mm depth below the epicardial surface. In analogy to cardiac tissue, one imaged surface of the optical phantom is denoted as epicardium (P) and the opposite surface as endocardium (N). Panels (a) and (b) show a diagrammatic representation of the phantom as well as the four images obtained in this case. The fluorescence amplitude is largest for the recordings taken from the epicardial surface (PP and NP) which is closest to the fluorescent sphere. Panel (c) shows a block diagram with the reconstructed depths Z_P, Z_N and Z_C compared to the true depths (dashed lines). Z_P is the most accurately reconstructed depth (0.1 mm error), but overall the reconstruction is extremely accurate with a 0.4 mm error on Z_C and 0.5 mm error on the diameter of the sphere (Z_N-Z_P).

B. Accuracy of the algorithm for varying depth and diameter

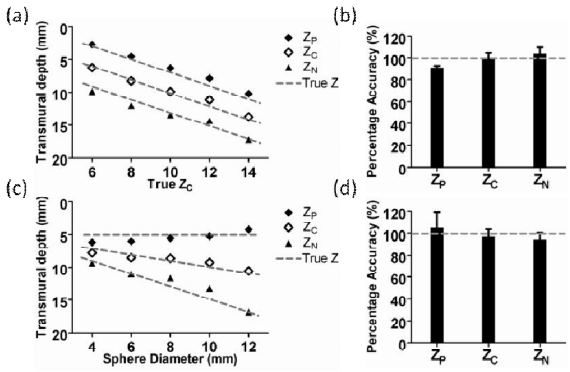

Fig. 3: Accuracy of the depth measurements for varying depths (a-b) and diameters (c-d) of the fluorescent sphere.

We tested the depth detection algorithm in optical phantoms for a wide range of depths and diameters of the fluorescent source. First, five optical phantoms were created each with a 6 mm diameter fluorescent sphere positioned at respective depths (Z_C) of 6, 8, 10, 12 and 14 mm below the P surface. Fig. 3(a) shows the reconstructed depths in each case, while Fig. 3(b) shows the mean accuracy of each measurement (Z_P, Z_C and Z_N). We find that irrespective of the depth of the source, the algorithm successfully reconstructs the depth of the fluorescent sphere with a mean error less than 14.9±7.2% and its thickness (Z_N-Z_P) with an accuracy of ±1.2 mm.

Secondly, we investigated the effect of varying the diameter of the sphere while keeping its distance to the P surface constant. Five optical phantoms were created in which a fluorescent sphere with respective diameters of 4, 6, 8, 10 and 12 mm was positioned at 5 mm from the P surface. Fig. 3(c) shows the results for each phantom, while Fig. 3(d) depicts the accuracy of the technique across all diameters. Again, we find that the method provides in each case accurate measurements of Z_P, Z_C and Z_N, with a mean error smaller than 8.8±6.4%. The estimation of the transmural diameter of the fluorescent source is found to be accurate within ±1.2 mm.

C. Depth detection in porcine ventricular preparations

The main purpose of the depth detection algorithm is its capability to accurately determine the intramural location of excitation sources and the intramural spread of excitation in myocardium. We next present preliminary results obtained in porcine left ventricular slabs (n=3). The slabs were paced at two different depths below the myocardium, and Z_P, Z_C,

and Z_N were determined as soon as a fluorescent signal of at least two times the noise amplitude could be detected in the two pairs of images. Fig. 4 shows the results of such an experiment. In this case, the left ventricular wall had a mean thickness of 12.7 mm and pacing was applied at a 5 mm depth below the epicardial surface. Panel (a) shows the four images recorded 21 ms after the initiation of the stimulus. The wave can clearly be observed in the PP, NP and PN images, but is faint in the NN image consistent with the pacing location closer to the epicardium and acquisition relatively shortly after the stimulus. The earliest frame in which the depth detection algorithm can be applied will provide the most accurate measure of Z_C. In this case we found it to be 4.9 mm, which is extremely close to the true stimulation depth of 5 mm in this case. Across all experiments we found ±1.6 mm accuracy in the determination of the depth of the source.

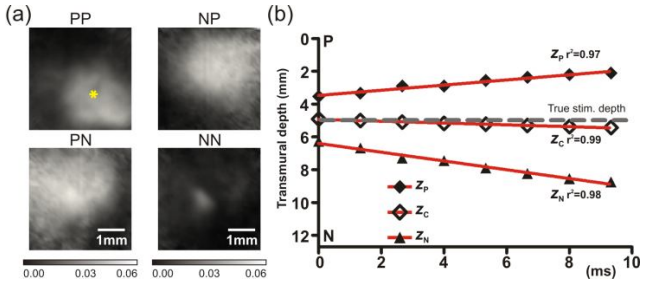

Fig. 4: Alternating illumination in porcine ventricular tissue. Panel (a) shows the four images obtained 21 ms after the stimulus and panel (b) shows the reconstructed depths as a function of time.

The subsequent frames in the acquisition can be used to measure the intramural expansion of the wave front by measuring Z_P and Z_N as a function of time. Panel (b) depicts this intramural spread. Overall the expansion of the wave front occurs at a nearly constant conduction velocity (excellent linear correlation between depth and time). The mean transmural conduction velocity that we measured was 21±12 cm/s. Although a trend of faster conduction towards the endocardium than the epicardium was observed, further experiments will be necessary to establish whether these differences are statistically significant.

IV. Discussion

In the present study we have experimentally evaluated the accuracy of a recently proposed method [6], based on AT imaging, in determining the depth of excitation sources in myocardium as well as the distance of the wave front to the epi- and endocardial surfaces (i.e. the transmural extent of the wave). Using optical phantoms we have shown that this non-destructive technique can provide the depth and diameter of fluorescent spheres irrespective of their depth in the phantom or diameter. Our depth estimates of fluorescent sources positioned over a range of 3-17 mm depths are accurate to ±1.2 mm despite predictions to incur greater error (up to 4 mm) with increasing depth [6]. Our preliminary studies in coronary-perfused ventricular wedge preparations indicate the feasibility of this technique in determining the excitation source and transmural extent and conduction velocity of excitation waves.

A previous experimental study had already validated the use of AT in determining the location of earliest intramural excitation with great accuracy in porcine ventricular preparations [7]. Our study goes one step further in providing not only an accurate location of the excitation site, but also in mapping the subsequent transmural propagation of the wave before it breaks through on the epi- and endocardial surfaces where it can be mapped by conventional means. Furthermore, our implementation of the AT imaging technique is different from the previous study in that it uses modulated LED illuminators which significantly simplifies the optical setup and does not require the use of opto-mechanical components such as beam choppers.

In conclusion, the non-destructive optical method presented here enables accurate determination of the depth and transmural extent of cardiac excitation waves. Although further validation will be required in tissue experiments, it represents a promising approach for the study of initiation and maintenance of lethal cardiac arrhythmias.

References

[1] P. B. Tabereaux, D. J. Dosdall, and R. E. Ideker, "Mechanisms of VF maintenance: wandering wavelets, mother rotors, or foci," *Heart Rhythm,* vol. 6, pp. 405-15, Mar 2009.

[2] M. Haissaguerre, M. Shoda, P. Jais, A. Nogami, D. C. Shah, J. Kautzner, T. Arentz, D. Kalushe, D. Lamaison, M. Griffith, F. Cruz, A. De Paola, F. Gaita, M. Hocini, S. Garrigue, L. Macle, R. Weerasooriya, and J. Clementy, "Mapping and ablation of idiopathic ventricular fibrillation," *Circulation,* vol. 106, pp. 962-7, Aug 20 2002.

[3] B. J. Caldwell, M. L. Trew, G. B. Sands, D. A. Hooks, I. J. Legrice, and B. H. Smaill, "Three distinct directions of intramural activation reveal nonuniform side-to-side electrical coupling of ventricular myocytes," *Circ Arrhythm Electrophysiol,* vol. 2, pp. 433-40, Aug 2009.

[4] D. A. Hooks, I. J. Legrice, J. D. Harvey, and B. H. Smaill, "Intramural multisite recording of transmembrane potential in the heart," *Biophys J,* vol. 81, pp. 2671-80, Nov 2001.

[5] O. F. Sharifov, R. E. Ideker, and V. G. Fast, "High-resolution optical mapping of intramural virtual electrodes in porcine left ventricular wall," *Cardiovasc Res,* vol. 64, pp. 448-56, Dec 1 2004.

[6] V. D. Khait, O. Bernus, S. F. Mironov, and A. M. Pertsov, "Method for the three-dimensional localization of intramyocardial excitation centers using optical imaging," *J Biomed Opt,* vol. 11, p. 34007, May-Jun 2006.

[7] B. G. Mitrea, B. J. Caldwell, and A. M. Pertsov, "Imaging electrical excitation inside the myocardial wall," *Biomed Opt Express,* vol. 2, pp. 620-33, 2011.

[8] I. Tachtsidis, L. Gao, T. S. Leung, M. Kohl-Bareis, C. E. Cooper, and C. E. Elwell, "A Hybrid Multi-Distance Phase and Broadband Spatially Resolved Spectrometer and Algorithm for Resolving Absolute Concentrations of Chromophores in the Near-Infrared Light Spectrum," *Oxygen Transport to Tissue Xxxi,* vol. 662, pp. 169-175, 2010.